LIMNOLOGY
and
OCEANOGRAPHY: METHODS

ASLO

Limnol. Oceanogr.: Methods 20, 2022, 222–232

doi: 10.1002/lom3.10482

Evaluating benthic flux measurements from a gradient flux system

Jeff Coogan,* **Jennie E. Rheuban, Matthew H. Long**
Department of Marine Chemistry and Geochemistry, Woods Hole Oceanographic Institution, Woods Hole, Massachusetts

Abstract

Multiple methods exist to measure the benthic flux of dissolved oxygen (DO), but many are limited by short deployments and provide only a snapshot of the processes occurring at the sediment–water interface. The gradient flux (GF) method measures near bed gradients of DO and estimates the eddy diffusivity from existing turbulence closure methods to solve for the benthic flux. This study compares measurements at a seagrass, reef, and sand environment with measurements from two other methods, eddy covariance and benthic chambers, to highlight the strengths, weaknesses, and uncertainty of measurements being made. The results show three major areas of primary importance when using the GF method: (1) a sufficient DO gradient is critical to use this method and is limited by the DO sensor precision and gradient variability; (2) it is important to use similar methods when comparing across sites or time, as many of the methods showed good agreement but were often biased larger or smaller based on the method; and (3) in complex bottom types, estimates of the length scale and placement of the DO sensors can lead to large sources of error. Careful consideration of these potential errors is needed when using the GF method, but when properly addressed, this method showed high agreement with the other methods and may prove a useful tool for measuring long-term benthic fluxes of DO or other chemical sensors or constituents of interest that are incompatible with other methods.

Measuring the benthic flux of chemical constituents is an important process for understanding benthic communities, sediment chemistry, and chemical budgets (Rowe et al. 1988; Middelburg and Levin 2009; Berg et al. 2022). To date, many benthic flux measurements are limited by short deployments or require lab analysis and provide only a snapshot of the processes occurring at the sediment–water interface. Developing improved methods that allow for longer deployment periods and increased accuracy is fundamental to closing chemical budgets, and advancing our understanding of processes associated with benthic communities and sediment biogeochemistry.

Dissolved oxygen (DO) fluxes are the focus of this methods paper, but regardless of the chemical being investigated, the benthic flux is due to a demand (or production) of a chemical at the seafloor that is supplied from (or released to) the overlying water column. This transfer of chemicals is limited by the physics associated with the bottom boundary layer (BBL) and results in a gradient based on

$$\text{Flux} = -K_{\text{DO}} \frac{dO}{dz}, \tag{1}$$

where O is the concentration of DO (the chemical concentration of interest in this study), z is depth, and K_{DO} is the eddy diffusivity that parameterizes the near bed turbulence. The eddy diffusivity controls the fate of near bed chemicals through the interaction of gradients with the overlying current. The BBL can be characterized by turbulent eddies that transfer the free stream momentum to a fixed boundary, the sea floor (Trowbridge and Lentz 2018). The near bed turbulent eddies are thus dependent on the free stream velocity, the distance off the bottom, and the bottom roughness. Benthic habitats of interest can modify the chemical demand as well as the bottom roughness (e.g., seagrasses, reefs) creating complex BBL dynamics. This interplay of biogeochemistry and overlying physics requires a detailed understanding of both driving forces to measure the fluxes occurring near the seafloor.

Because of these challenges and the importance of measuring the benthic flux, multiple methods exist to measure it: in situ chambers (Tengberg et al. 2004), eddy covariance (EC) (Berg et al. 2022), calculating the flux based on observed gradients (McGillis et al. 2011), in situ profiles (Rabouille et al. 2003), and ex situ sediment core incubations (Kuriyama et al. 2021). One of the simplest of these methods is to measure the benthic flux with a chamber that allows for the production or respiration rates to be calculated based on the rate

*Correspondence: jcoogan@whoi.edu

change inside the chamber. A drawback of this method is it modifies the hydrodynamics and chemical environment inside the chamber. Efforts have been made to improve chamber designs to account for these challenges and improve the benthic flux measurements (Glud 2008). Modifications have included adding motors to mix the water in the chamber, flexible walls, and tracer additions (Tengberg et al. 1995).

A second method, the EC method, solves the instantaneous flux of DO as

$$\text{Flux} = \overline{O'w'}, \tag{2}$$

where w is the vertical velocity and primes and overbars denote the turbulent components and Reynolds averages. The method has been used in a number of benthic habitats including benthic macrophytes (Hume et al., 2011; Rheuban et al., 2014), oyster beds (Reidenbach et al., 2013; Volaric et al., 2018), and coral reefs (Long et al. 2013; Rovelli et al. 2015). Major challenges include waves and scale of the DO fluxes are sufficiently large to resolve the oxygen variance. Long (2021) developed improved analysis techniques to address these challenges and improve measurements of the benthic flux for the EC method.

A third method, the gradient flux (GF) method, is the focus of this study and solves Eq. 1 by measuring the gradient and estimating the eddy diffusivity. Following McGillis et al. (2011) the eddy diffusivity in Eq. 1 can be solved as

$$K_{\text{DO}} = u_* \kappa l, \tag{3}$$

where u_* is the friction velocity, κ is the von Karman constant, and l is the turbulent length scale. Fluxes have been measured in reef environments with this method (McGillis et al. 2009, 2011; Turk et al. 2015; Takeshita et al. 2016; Platz et al. 2020), but a major challenge is accurately solving the eddy diffusivity term. The GF method is advantageous because it can use slower response sensors when compared to the EC method that requires specialized fast sensors that only exist for a few variables (DO, pH, temperature, salinity). The use of less specialized sensors can expand the chemical fluxes that can be measured, advance long-term measurement capabilities and expand the number of researchers able to make these measurements.

The focus of this study is to evaluate the GF method and determine the best way to solve for the eddy diffusivity term. Measurements from a seagrass, reef, and sand environment provide a range of benthic habitats to allow for a comparison of these methods that can highlight the strengths, weaknesses, and uncertainty of measurements being made. The results are compared with the two other methods: the benthic chamber method and the EC method. All these methods have been previously used to solve the benthic flux, and the aim of this paper is to better understand the physics and error associated with the GF method and provide guidance for future DO work and other chemical constituents of interest with these methods.

Methods

Study site characteristics

Three sites in the Florida Keys (Fig. 1) were used for this research to provide a range of bottom characteristics over which the data could be analyzed, and more detail on the three sites can be found in Long (2021). The sites included a seagrass site, a reef site, and a sand site (Fig. 2). The three sites were separated by an average distance of 300 m. The general region is located on the outer reef of the Florida Keys near Key Largo, ~7 km offshore. The reef site was dominated by octocorals, algae, and rubble (Hopkinson et al. 2020; Owen et al. 2021). The seagrass site was predominantly *Thalassia testudinum* (turtlegrass) with a canopy height of 0.2 m. The sand site consisted of carbonate sands with 0.1 m bedforms. Data was collected from 21 to 28 June, 2018, over two deployment periods. Each site had an EC system and GF system to measure the benthic flux of DO. The sand and seagrass sites also had benthic chamber deployments to provide additional measurements of the benthic flux.

Benthic chamber method

The benthic chamber method consisted of a clear 20 cm diameter by 31 cm tall plexiglass chamber that was inserted 15 cm into the sand and seagrass to directly measure the change in DO in the chamber. Each chamber had a stirring motor that rotated at 44 rpm to mimic the natural flow dynamics occurring outside the chamber. The chambers were deployed by divers to ensure proper placement. After 90 min, a water sample was extracted and DO was measured

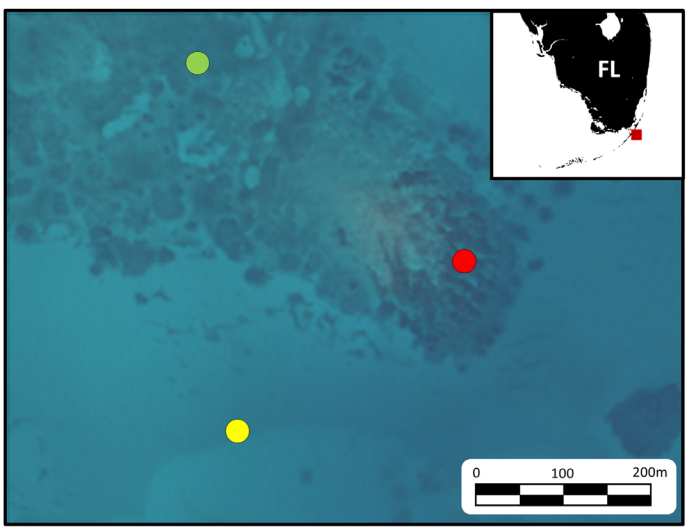

Fig. 1. Deployment locations for the seagrass (green), reef (red), and sand (yellow) sites in the Florida Keys 7 km offshore from Key Largo. Satellite image from National Geodetic Survey (2021).

immediately on the boat with a PyroScience GO2 DO optode. This method allowed for the benthic flux to be calculated directly from the change in DO that occurred in the chamber and has been previously used in a number of studies to calculate the benthic flux (Hall et al. 1989; Jahnke et al. 2000; Herzfeld et al. 2001; Long et al. 2015). A major limitation of the method was it provided only point measurements for comparisons. Three measurements were made at the sand site and two measurements were made at the seagrass site. This method was not used at the reef site due to the solid reef structure that would not allow for insertion of the chamber.

EC method

The EC method used an eddy covariance hydrogen ion and oxygen exchange system (ECHOES) to measure the benthic flux. The ECHOES was comprised of an acoustic Doppler velocimeter (ADV) and FireStingO_2 Mini fiber-optic DO meter with a fast-response (~ 0.3 s) 430 μm diameter optode (PyroScience). ECHOES was designed to align itself into the flow and used a microfluidic pump system to pump water past the DO sensor. More details about the ECHOES design can be found in Long et al. (2015, 2019). Deployment lengths were on average 4.5 d and were deployed by divers to ensure level and steady placement on the various bottom types. The sampling heights are presented in Table 1. The ECHOES measured the direct covariance of DO and vertical velocity to calculate the benthic flux of oxygen (Eq. 2). ADV velocities were omitted when the correlation was < 50. If > 10% of the ADV burst were omitted the data was not included in analysis. Due to waves biasing the covariance measurements, a cross-power spectral density (CPSD) method was used to transform the data into frequency space where data outside the wave frequencies could be separated from the signal and used to calculate the benthic flux. Following Long (2021), the CPSD can be solved as

$$\text{Flux} = \sum_{f_1}^{f_2} P_{w'O'}(f)df, \tag{4}$$

where $P_{w'O'}(f)$ is the CPSD of the vertical velocity and DO as a function of frequency summed from f_1, the burst length, to f_2, the cut-off frequency. The burst length was 15 min for all the ADVs in this study, and the cut-off frequency was solved for each burst length as $1/(2T_d)$ where T_d is the dominant wave period. Data were further omitted when waves impacted the spectral calculation defined by Rosman and Gerbi (2017) as $\frac{\sigma_w}{U} < 2$ and $\frac{\sigma_w k_0}{\omega_w} < 0.5$ where σ_w is the wave velocity, ω_w is the peak frequency, and k_0 is the roll-off wave number. These criteria mark periods where the waves can modify the turbulent spectra outside of the wave band, and omitting the wave frequency from the CPSD and dissipation estimates is not sufficient to fully omit the wave orbital influence. A storage term was also included following Rheuban et al. (2014) to account for changes in DO concentration below the ADV sensor.

GF method

The GF system consisted of a single Seabird SeapHOx connected to two pumps with intakes roughly 1 m apart (Table 1 list the exact pump heights) that alternated pumping water

Fig. 2. GF measurement platform showing examples of the three different bottom types examined in this study (**a**) sand, (**b**) seagrass, and (**c**) reef.

Table 1. Site measurement characteristics in meters for the deployment of the eddy covariance hydrogen ion and oxygen exchanged system (ECHOES), gradient system intakes and associated roughness elements and depth.

Site	ECHOES height	Gradient height 1	Gradient height 2	Roughness length	Depth
Reef	0.97	0.24	1.15	0.5	2.9
Grass	0.55	0.22	1.10	0.2	4.8
Sand	0.35	0.15	1.08	0.1	6.3

continuously past a sensor every 15 min, resulting in a full pump cycle of 30 min. The sensor took 100 samples over the last 5 min of each 15-min period, similar to designs used previously by Takeshita et al. (2016). The surface and bottom measurements were then linearly interpolated to the same time points which allowed for the DO gradient to be measured every 30 min. In addition to the gradient system, a Nortek Aquadopp HR collected current data every 15 min throughout the water column with a 90 s burst sample at 1 Hz over 2 cm bins. Finally, the ADV from the ECHOES was used to collect high frequency (16 Hz) velocity data. The same quality control used for the EC methods was applied to the velocity data for the GF method.

The gradient and velocity data were then used to solve Eq. 1 and investigate multiple approaches for solving the eddy diffusivity term (K_{DO}). The first method solved the eddy viscosity

$$K_M = \frac{(\overline{u'w'})}{du/dz}, \tag{5}$$

where K_M is the turbulent diffusion of momentum, $\overline{u'w'}$ is the Reynolds stress, and u is the horizontal velocity. The CPSD approach outlined for the EC method was also used to solve the Reynolds stress ($\overline{u'w'}$) and replaces the O' term with u' in Eq. 4. The vertical current shear was calculated from the Aquadopp data. The eddy viscosity was then related to the DO eddy diffusivity with a turbulent Schmidt number (Sc) of 1 where

$$Sc = \frac{K_M}{K_{DO}}, \tag{6}$$

where K_M is the turbulent diffusion of momentum and K_{DO} is the turbulent diffusion of DO.

The remaining methods solved for K_{DO} based on a linear scaling of diffusivity with depth (e.g., McGillis et al., 2011; Takeshita et al. 2016; Eq. 3). The friction velocity was solved using three different methods: a log profile fit (log fit method), solving directly for the Reynolds stress (covariance method), and from the turbulent dissipation (dissipation method). In fully turbulent boundary layers, the velocity profile takes the shape of a logarithmic profile and the friction velocity can be solved using the Karman–Prandtl equation

$$u_* = \frac{\kappa U(z)}{\log(z/z_0)}, \tag{7}$$

where U is the velocity, and z_0 is the roughness scale. The covariance method for solving the friction velocity was solved directly from the reynolds stress

$$u_* = \sqrt{\overline{u'w'}}, \tag{8}$$

where $\overline{u'w'}$ is solved in the same manner as the eddy viscosity equation using the CPSD. This provides the most direct estimate of the bottom stress. The third approach, dissipation method, assumes that the shear production due to the bottom stress is balanced by the turbulent dissipation and can be solved as

$$u_* = \sqrt[3]{\varepsilon \kappa z}, \tag{9}$$

where ε is turbulent kinetic energy dissipation rate solved based on fitting the data to the Kaimal et al. (1972) spectral model. Following Scully et al. (2011) the one sided wavenumber k autospectra of the turbulent vertical velocity fluctuations can be modeled as

$$\frac{kS_{ww}(k)}{\langle w'^2 \rangle} = \frac{0.16(k/k_o)}{1+0.16(k/k_o)^{5/3}}, \tag{10}$$

where S_{ww} is the vertical velocity autospectra, k is the wavenumber, and k_o is the wavenumber associated with the dominant energy containing scales. From this, dissipation can be solved as

$$k_o = \alpha^{3/2} \frac{\varepsilon}{\langle w'^2 \rangle^{3/2}}, \tag{11}$$

where α is the Kolmogorov constant (0.68).

Equations 7–9 were then used to solve Eq. 3 providing three different methods to solve for the diffusivity. The length scale, l, from Eq. 3 was also examined four different ways: based on the distance off the bottom (McGillis et al. 2011), calculated based on Eq. 11 as a function of k_o (Scully et al. 2011), calculated as a function of momentum closure from Eqs. 5 and 3 with respect to the eddy viscosity, and calculated as a function of the EC method and DO gradient combining Eqs. 1–3. From these equations the best method for solving diffusivity and GF method was evaluated across a range of gradients, bottom types, and wave conditions. A storage term was also included following Rheuban et al. (2014) to account for changes in DO concentration below the ADV sensor that are part of the benthic flux.

Assessment

DO gradient

All the sites had a diurnal DO signal that peaked in the afternoon and was lowest at dawn (Fig. 3). The DO gradient also exhibited a diurnal response, where positive gradients (bottom-top) occurred during the day and negative gradients occurred at night due to net benthic oxygen production during the day and net benthic oxygen demand at night. The reef site had an average net gradient of −2.8 mmol O_2 m^{-4} indicating it was net heterotrophic during the deployment period. In

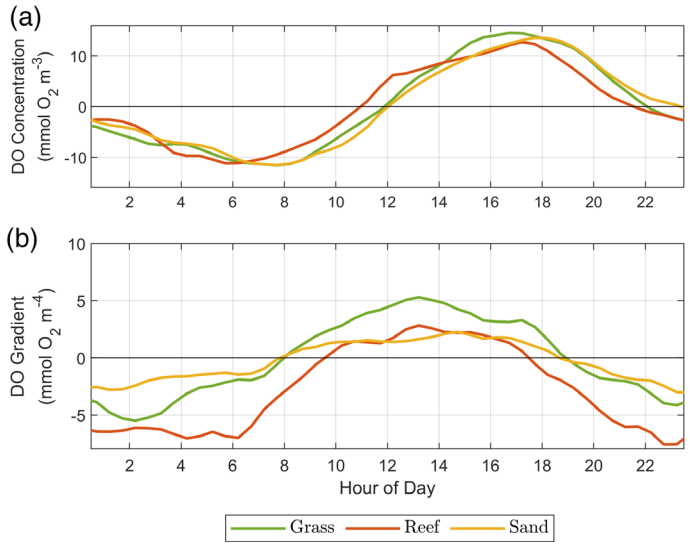

Fig. 3. Dissolved oxygen patterns for (**a**) deviations of the DO concentration from the deployment mean and (**b**) gradient changes averaged over 24 h at the three different sites: Reef (red), sand (yellow), seagrass (green).

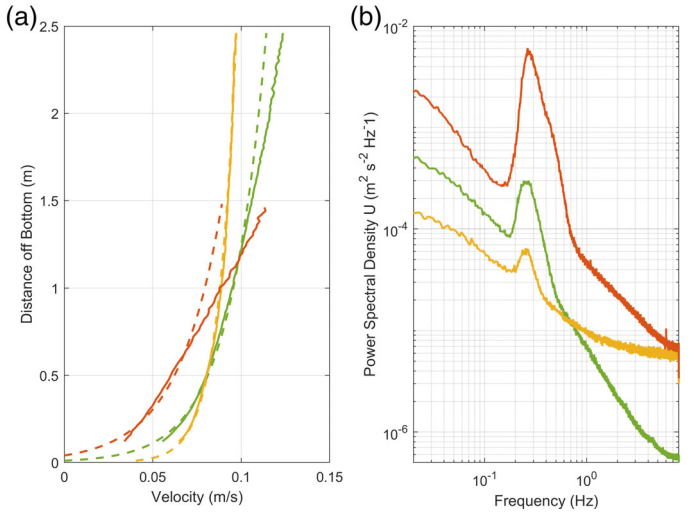

Fig. 4. Hydrodynamic data for the reef (red), sand (yellow), and seagrass (green) sites showing (**a**) the near bed average current profiles (solid line) and log fit profile (dashed line) for all the data and (**b**) average PSD of velocity over the whole deployment.

comparison the seagrass and sand sites net gradient was closer to zero but were also both negative with values of −0.1 and −0.3 mmol O_2 m^{-4}, respectively. Both the seagrass and reef sites had a measurable average absolute gradient of 3.1 and 4.0 mmol O_2 m^{-4}, respectively. The sand site in comparison had a lower average absolute gradient of 1.6 mmol O_2 m^{-4}. Since a gradient is needed to solve Eq. 1, ensuring the gradient exceeds the instrument noise floor is critical to calculate the benthic flux.

Bottom stress

The three sites had relatively similar velocities outside of the BBL with average velocities around 10 cm s^{-1} (Fig. 4). The friction velocity was greatest at the reef site where the average value based on covariance was 0.012 m s^{-1} compared with 0.005 and 0.004 m s^{-1} for the seagrass and sand sites, respectively. The larger friction velocity was due to the increased roughness at the reef site. This increased roughness is also evident in the roughness scale (z_o) from Eq. 7 that was 4 cm at the reef site, 1 cm at the seagrass site and 0.2 cm at the sand site. Comparing methods for solving the friction velocity (Eqs. 7–9) showed a range of trends among sites and methods. The sand site was the most consistent among the three methods with the lowest root mean square error (RMSE) with respect to the covariance measurement and smallest difference between the plots in Fig. 5. The biologically complex bottom sites (seagrass and reef) had larger RMSE when comparing the three methods.

The log profile method (Eq. 7) provided better (lower RMSE) fits at the sand site but poorer fits (higher RMSE) for the reef and seagrass sites when compared to the dissipation method. Figure 4 shows the average current profile and corresponding log fit. The comparisons of friction velocity estimates showed the limitation of the log profile fits where waves and upstream dynamics can heavily bias the resulting stress calculation that is not apparent when solving the fit and looking at the log profile. Figure 4b shows the wave energy at the three sites and is a result of the depth of the site where the shallowest site (reef) had the greatest wave impacts.

Length scales

Table 2 shows the length scale, *l*, from Eq. 3 that used four separate methods based on ADV distance off the bottom, momentum closure, Kaimal, and DO closure with the EC method to solve for this value. Table 2 also shows the ADV distance to the canopy/bedform. All of the measured distances off the bottom showed poor agreement with the momentum and DO flux-based length scales. At all three sites, the ADV distance off the bottom and ADV distance to canopy were both larger than the other three length scale estimates. This highlights the challenge in measuring the length scale as the traditional distance off the bottom or distance to the canopy in complex bottom types. The three sites had a range of hard and flexible materials that make up the canopy and seafloor and modify the turbulent dynamics. The seagrass and sand site had the best agreement (< 5 cm) between the momentum, Kaimal, and EC flux length scale when compared to the reef site. The reef had a range of length scales based on the method, but comparable values for the Kaimal and momentum closure methods. Based on this, the momentum closure

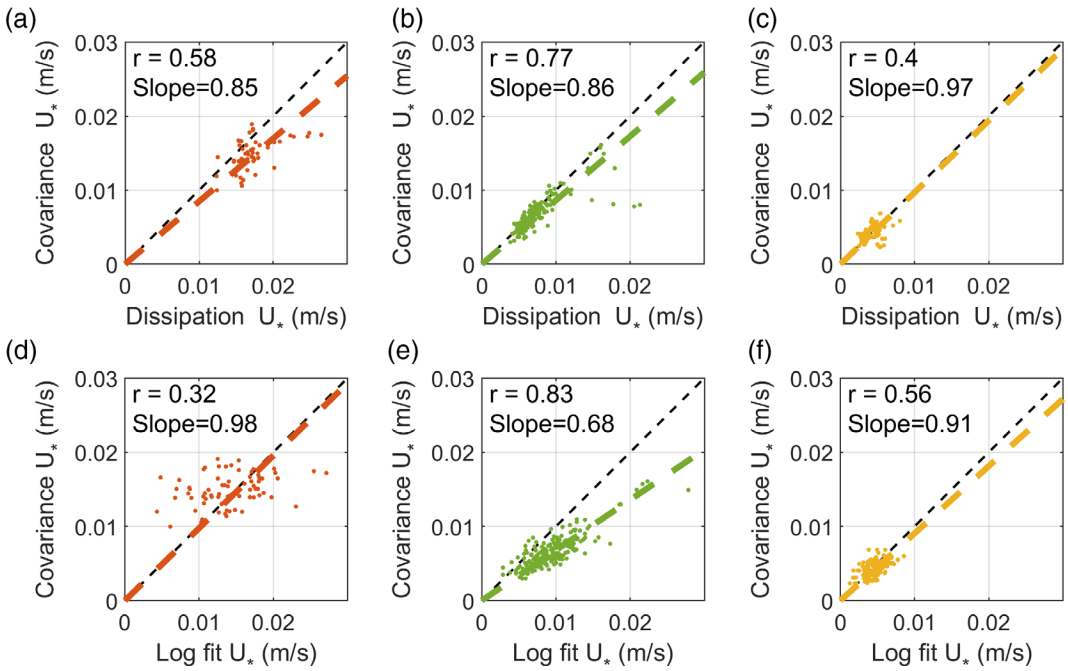

Fig. 5. Comparison of covariance friction velocity with dissipation estimates (**a–c**), and log fit estimates (**d–f**) for the reef (red), seagrass (green), and sand (yellow) sites. Black dashed lines are the 1:1 slope and colored dashed lines are the best fit with the *r* value and slope reported.

Table 2. Length scale estimates for l in Eq. 3 with respect to the ADV height for each site across four methods where lengths are in m.

	ADV distance off the bottom	ADV distance to canopy/ bedform	Momentum closure	Kaimal roll-off length scale	EC flux closure
Reef	0.97	0.47	0.40	0.42	0.30
Grass	0.55	0.35	0.22	0.18	0.23
Sand	0.35	0.25	0.12	0.12	0.17

was used as the length scale for solving Eq. 3 and calculating the DO eddy diffusivity.

Benthic flux and eddy diffusivity

The benthic flux based on the EC method (Eq. 4) ranged from 16.0 to −47.7 mmol O_2 m^{-2} h^{-1} across all sites over the course of the deployment periods (Fig. 6). The reef was net heterotrophic with an average daily benthic flux of −302.4 mmol O_2 m^{-2} d^{-1} and the sand and seagrass sites were net autotrophic with an average benthic flux of 21.6 and 36.0 mmol O_2 m^{-2} d^{-1}, respectively (note these values differ from Long, 2021 due to a greater number of measurement days in this study). In comparison, across all GF methods fluxes ranged from 146.1 to −96.2 mmol O_2 m^{-2} h^{-1}. On average the reef, seagrass, and sand sites were all heterotrophic with an average daily benthic flux of −540.0, −12.0, and −7.2 mmol O_2 m^{-2} d^{-1}, respectively.

The four GF methods were compared with the EC method using the calculated flux (Fig. 6) and a direct estimate of diffusivity based on the EC flux divided by the DO gradient (Table 3). The GF methods at the sand site had the best agreement across all methods, but were largely driven by changes in near bed DO (storage term) and not the vertical exchange component due to the low DO gradients at that site. The log fit had the best fit with respect to the EC method (RMSE of 1.5) and the eddy viscosity was the poorest (RMSE 2.2) at the sand site. The benthic chambers also had good fits with a similar RMSE between all the methods (RMSE 0.9–1.7).

The seagrass site had the log fit being the poorest fit (RMSE of 6.5), eddy viscosity being the best fit (RMSE 5.1) and variability through time for all methods with respect to the EC method. On 28 June, a large deviation between the EC method and the GF methods occurred; this deviation was associated with a period of thermal stratification. The stratification likely impacted the BBL dynamics and violated the assumptions of the GF method resulting in an overprediction of respiration during this period. The chamber data had lower production at the seagrass site in comparison to all the methods (RMSE 4.5–11.8).

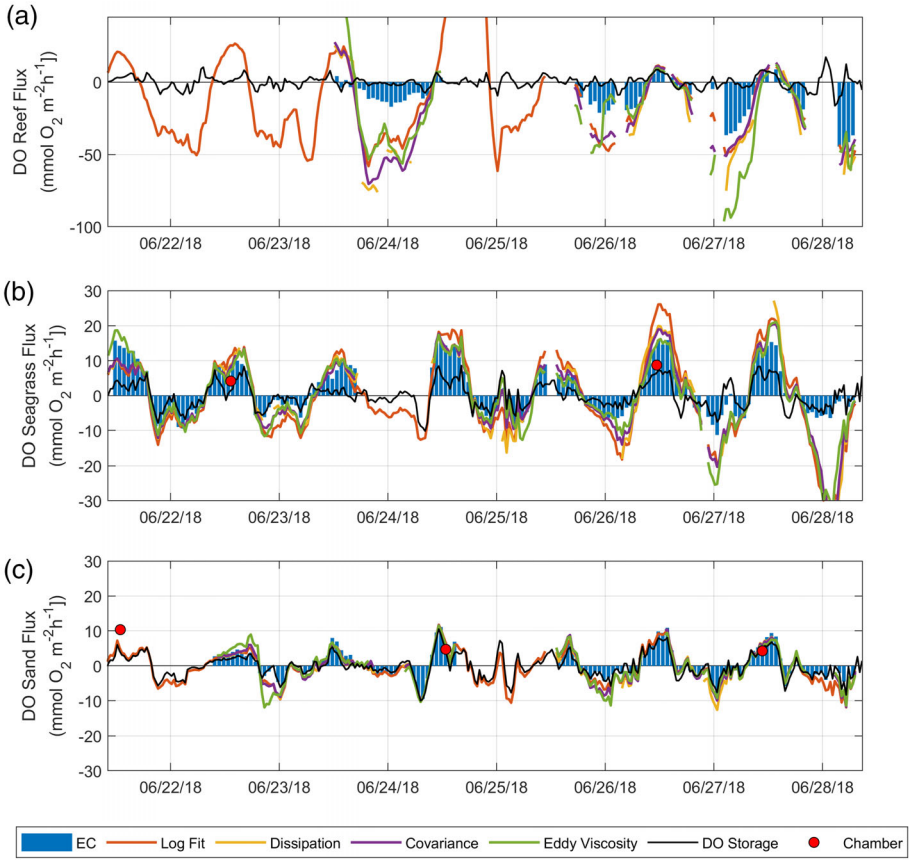

Fig. 6. Time series of flux measurements from the Florida keys (**a**) reef, (**b**) seagrass, and (**c**) sand site. Measurements of the DO flux are shown as blue bars for the eddy covariance system, red dots for the chamber system, and the gradient method is solved with four different estimates of eddy diffusivity: Log profile (red), dissipation (yellow), covariance (purple), and eddy viscosity (green). The DO storage term is plotted as a black line. Note differences in *y*-axis scales between sites.

Table 3. Eddy diffusivity $m^2\ s^{-1}$ calculations for each of the four methods and a direct estimate based on the EC method and observed gradient.

	EC direct	Log fit	Dissipation	Covariance	Eddy viscosity
Reef	9.2×10^{-4}	1.7×10^{-3}	2.8×10^{-3}	2.0×10^{-3}	2.3×10^{-3}
Seagrass	5.0×10^{-4}	7.6×10^{-4}	6.7×10^{-4}	5.1×10^{-4}	5.2×10^{-4}
Sand	1.8×10^{-4}	2.1×10^{-4}	2.1×10^{-4}	2.1×10^{-4}	2.4×10^{-4}

The reef had the largest variability between the EC method and the GF methods. The reef had dissipation being the poorest fit (RMSE of 28.3) and log being the best fit (RMSE 16.6). The large variability between the EC and GF methods could also be seen in the eddy diffusivity data where Table 3 highlights the diffusivity based on solving directly was $9.2 \times 10^{-4}\ m^2\ s^{-1}$ and all the other methods were order of magnitude 10^{-3}.

Discussion

Measuring the DO gradient

A key component of the GF method is to measure a sufficient DO gradient (greater than the instrument and background noise) while staying within the BBL. The sand site gradient often fell below the instrument accuracy ($\pm$ 3 mmol m^{-3}) and presents a limit for the application of the GF method when using the SBE 63 Optical Dissolved Oxygen Sensor. To help facilitate robust gradient measurements, a single instrument with two pump heights was used to eliminate errors due to intercalibration between multiple instruments. With this single sensor approach, measuring the gradient is limited by the precision of the DO sensor. Natural variability in the gradient can also impact measurements. In this study, the average standard deviation over each 5 min burst sample for the entire deployment was 0.4, 0.5, and 2.1 mmol m^{-3} at the sand, seagrass, and reef site, respectively. This standard

deviation is a function of the instrument noise and natural background variability, where the reef has the highest variability due its rough irregular bottom and higher levels of mixing. With highly variable sites, longer burst sampling can be used to capture and average the natural variability for each site and improve gradient measurements. However, longer sampling times present a tradeoff if the sampling length increases the time between surface and bottom measurements. In this situation, the interpolation of the oxygen concentration to sync up the pumping heights in time can become an additional source of error as the gradient may also be changing in time, especially at periods of dynamic changes in physical drivers such as dusk or dawn and during tidal changes. The DO gradient that develops near the sea floor is due to a balance of the oxygen consumption/production and the eddy diffusivity where Eq. 1 can be rewritten as

$$\frac{dO}{dz} = \frac{\text{Flux}}{K_{\text{DO}}}. \tag{12}$$

This equation can be used prior to fieldwork to estimate if a sufficient gradient will occur at a study site. The flux can be estimated based on previous studies and site characteristics. K_{DO} can be estimated from a quadratic drag equation

$$K_{\text{DO}} = C_{\text{d}} U_{\text{bottom}} \kappa z, \tag{13}$$

where U_{bottom} is the near bed velocity and C_{d} is a site dependent drag coefficient that can be estimated for sand (Ribberink 1998), reefs (Lentz et al. 2017), and seagrass (Nepf, 2012). From this relationship estimates of the expected gradient can be compared to instrument accuracy and determine if the gradient method is applicable at a site. This method can also evaluate other chemical constituents in place of oxygen. Caution should be used when measuring closer to the seafloor (decreasing K_{DO}) in an effort to increase the gradient and make it easier to resolve. The turbulent regime can change within the canopy leading to divergent flows that deviate from a fully developed BBL, and very close to the bed the turbulence can transition to a viscous sublayer. In practice, the height of the bottom gradient measurement should be at least at or above the largest bottom roughness length.

Length scale

The second key component of this method is the length scale in Eq. 3. This variable is the same order of magnitude as the DO gradient and can have a large impact on the magnitude of the resulting flux calculations. The length scale has previously been set as the distance off the bottom (McGillis et al. 2011), but this may not accurately capture the turbulent length scale at sites with flexible materials that dampen turbulence (seagrass), large irregular stiff and flexible objects (reef), and shifting bottom features (sand bedforms). Because of the term's first order importance, multiple methods should be employed to examine the correct length scale for a site. Takeshita et al. (2016) used a displacement height and integration constant as tuning parameters to account for this length scale difference from the distance off the bottom. In this study, solving the momentum balance results in values that closely match the eddy viscosity ($Sc = 1$). This method worked well at the seagrass site where similar values were observed across the momentum, Kaimal, and EC closure methods. With a length scale based simply on distance off the bottom (e.g., McGillis et al. 2011) absolute flux values were 60% greater than those using the momentum closure.

At the reef site, adjusting the length scale based on momentum was not enough to improve the measurement accuracy for the GF method. The difference between the EC flux closure and momentum closure was due to the flux being calculated over the DO gradient, where the lower pump height was likely within the reef canopy (Fig. 2), suggesting it was in a different turbulent regime than the ADV. In the canopy, the flow encounters increased drag as it moves around coral branches and fans generating wakes and turbulence at the scale of canopy elements (Davis et al. 2020). The GF calculation assumes there is a linear gradient between the two DO measurement heights and this may not be valid as the flow transitions from within the reef canopy to within the BBL. This requires a modified scaling of l between the two pump heights or placing the lower pump further off the bottom and should be the focus of future work. Each approach has a tradeoff, a more complex scaling argument can be difficult to solve and raising the lower pump height will reduce the DO gradient making it harder to measure.

Calculating eddy diffusivity and benthic flux

The eddy diffusivity terms calculated in this study (Table 3) were based on a direct solution from the EC method, measurements of the eddy viscosity, and a simple length scale argument that relates shear production to the length scale of turbulence via the von Karman constant (Eq. 3). This study examined multiple ways to calculate the shear production term U_* based on: a log profile (Eq. 7), measuring the Reynolds stress from covariance (Eq. 8), and turbulent dissipation (Eq. 9). Dissipation had the poorest fit with respect to the EC method across all the sites. This poor fit was most evident at the reef site where multiple measurements exceed the plot range (Fig. 6a). A key assumption in the dissipation estimates are that shear production and dissipation are balanced. Reidenbach et al. (2006) found good agreement for this at a reef site in the Red Sea but noted waves were insignificant at their study site. Waves present a major limitation of all the measurements. The covariance and dissipation measurement took advantage of spectral analysis to remove the wave frequencies. However, removing the wave frequencies may still bias the measurements (Rosman and Gerbi, 2017; Long 2021). Rosman and Gerbi (2017) have showed when $\frac{\sigma_w}{U} < 2$ and

$\frac{\sigma_w k_0}{\omega_w} < 0.5$ waves can modify the turbulent spectra outside of the wave band and bias measurements. In addition, close to and within the reef canopy production and dissipation may not be balanced as wakes from irregular upstream objects may be advected past the ADV. Similarly, at the seagrass site, dissipation from the seagrass canopy may impact the dissipation–production balance. This dissipation and canopy influence also resulted in poor fits for the log profiles. Nepf (2012) found that at twice the canopy height the velocity profile is logarithmic but closer to the bed the canopy interaction results in poor fits.

Sherwood et al. (2006) looked at similar comparisons of u_* across the three methods (Eqs. 7–9) used in this study on the Washington coast and notes that though the values of the three methods agreed reasonably well, there are important systematic differences and the methods are not equivalent for comparisons among sites. Similarly, benthic flux comparisons should make note of the methods used where the log profile had on average higher u_* measurements at the seagrass site and thus greater fluxes. Kim et al. (2000) found similar agreement among methods in the York River estuary but that the covariance (Eq. 8) provided better estimates close to the bed, and the log profile was the most variable due to sensitivity to stratification and thickness of the constant stress layer.

The eddy viscosity measurements had the benefit of not needing the length scale to be estimated, and spectral techniques could remove the wave bias resulting in good agreement at the sand and seagrass sites. Holtappels and Lorke (2011) found the use of the eddy viscosity was limited when current gradients were close to zero. This presents a limit of the viscosity measurement where slow currents and low velocity gradients during slack tides can result in less mixing and larger DO gradients. This means the two gradients can be out of phase and result in problematic measurements when both gradients need to be measured at a threshold greater than instrument noise. The eddy viscosity measurements were made from a point near the middle of the two heights that were used to solve the DO gradient. When the eddy viscosity does not change linearly between the two pump heights this can result in poor estimates with this method. This occurred at the reef where the lower DO value was measured at 0.24 m off the bottom and the ADV was 0.97 m off the bottom and resulted in eddy viscosity measurements being made outside the reef canopy but gradients being measured across the reef canopy. Adding a second ADV to measure the turbulent dynamics at the lower height measurement may provide improved measurements for future flux calculations.

Conclusion

The three major measurement parameters that are critical to the GF method for calculating the DO flux are the DO gradient, estimates of the friction velocity, and estimates of the length scale. Each of the sites highlights a different component of these challenges when using the GF method. The sand site has low DO gradients which is a fundamental component to measure the flux. The seagrass site has length scales that are modified by the seagrass canopy and need to be corrected. The reef site has poor fits with the eddy viscosity and Eq. 3 methods which was due to one of the DO pump heights being in the reef canopy. This can be corrected with the EC data but requires knowledge of the benthic flux to perform this correction. Careful consideration of these potential errors is needed when using the GF method, but when properly addressed the GF method showed high agreement with both the EC method and the benthic chamber method. When compared to the EC method, the GF approach provides a useful tool for low flows (small turbulent fluxes) that are difficult to measure with the EC approach. Both methods though need fully developed turbulence and measurements in the BBL for these techniques to be applied. The data highlights that the GF method can be a useful tool for measuring long-term benthic fluxes of DO or other chemical constituents of interest where slower sensors or discrete water samples can be used with this gradient approach to calculate the benthic flux

Data availability statement

Data for this study are archived at the Biological & Chemical Oceanography Data Management Office per NSF policies (https://www.bco-dmo.org/person/560155).

References

Berg, P., M. Huettel, R. N. Glud, C. E. Reimers, and K. M. Attard. 2022. Aquatic eddy covariance: The method and its contributions to defining oxygen and carbon fluxes in marine environments. Ann. Rev. Mar. Sci. **14**: 431–455. doi:10.1146/annurev-marine-042121-012329

Davis, M., K. A. Davis, G. Pawlak, and S. G. Monismith. 2020. Turbulence and coral reefs. Ann. Rev. Mar. Sci. **13**: 343–373. doi:10.1146/annurev-marine-042120-071823

Glud, R. N. 2008. Oxygen dynamics of marine sediments oxygen dynamics of marine sediments. Mar. Biol. Res. **4**: 243–289. doi:10.1080/17451000801888726

Hall, P. O. J., L. G. Anderson, M. M. R. van der Loeff, B. Sundby, and S. F. G. Westerlund. 1989. Oxygen uptake kinetics in the benthic boundary layer. Limnol. Oceanogr. **34**: 734–746. doi:10.4319/lo.1989.34.4.0734

Herzfeld, M., D. P. Hamilton, and G. B. Douglas. 2001. Comparison of a mechanistic sediment model and a water column model for hindcasting oxygen decay in benthic chambers. Ecol. Model. **136**: 255–267. doi:10.1016/S0304-3800(00)00429-4

Holtappels, M., and A. Lorke. 2011. Estimating turbulent diffusion in a benthic boundary layer. Limnol. Oceanogr.: Methods **9**: 29–41. doi:10.4319/lom.2011.9.29

Hopkinson, B. M., A. C. King, D. P. Owen, M. Johnson-Roberson, M. H. Long, and S. M. Bhandarkar. 2020. Automated classification of three-dimensional reconstructions of coral reefs using convolutional neural networks. PLoS One **15**: e0230671. doi:10.1371/journal.pone.0230671

Hume, A. C., P. Berg, and K. J. McGlathery. 2011. Dissolved oxygen fluxes and ecosystem metabolism in an eelgrass (*Zostera marina*) meadow measured with the eddy correlation technique. Limnol. Oceanogr. **56**: 86–96. doi:10.4319/lo.2011.56.1.0086

Jahnke, R. A., J. R. Nelson, R. L. Marinelli, and J. E. Eckman. 2000. Benthic flux of biogenic elements on the southeastern US continental shelf: Influence of pore water advective transport and benthic microalgae. Cont. Shelf Res. **20**: 109–127. doi:10.1016/S0278-4343(99)00063-1

Kaimal, J. C., J. C. Wyngaard, Y. Izumi, and O. R. Coté. 1972. Spectral characteristics of surface-layer turbulence. Q. J. R. Meteorol. Soc. **98**: 563–589. doi:10.1002/qj.49709841707

Kim, S. C., C. T. Friedrichs, J. P. Y. Maa, and L. D. Wright. 2000. Estimating bottom stress in tidal boundary layer from acoustic Doppler velocimeter data. J. Hydraul. Eng. **126**: 399–406. doi:10.1061/(ASCE)0733-9429(2000)126:6(399)

Kuriyama, K., S. Gründling-Pfaff, N. Diehl, J. Woelfel, and U. Karsten. 2021. Microphytobenthic primary production on exposed coastal sandy sediments of the southern Baltic Sea using ex situ sediment cores and oxygen optodes. Oceanologia **63**: 247–260. doi:10.1016/j.oceano.2021.02.002

Lentz, S. J., K. A. Davis, J. H. Churchill, and T. M. DeCarlo. 2017. Coral reef drag coefficients - water depth dependence. J. Phys. Oceanogr. **47**: 1061–1075. doi:10.1175/JPO-D-16-0248.1

Long, M. H. 2021. Aquatic biogeochemical eddy covariance fluxes in the presence of waves. J. Geophys. Res. Oceans **126**: e2020JC016637. doi:10.1029/2020jc016637

Long, M. H., P. Berg, D. de Beer, and J. C. Zieman. 2013. In situ coral reef oxygen metabolism: An eddy correlation study. PLoS One **8**: e58581. doi:10.1371/journal.pone.0058581

Long, M. H., M. A. Charette, W. R. Martin, and D. C. Mccorkle. 2015. Oxygen metabolism and pH in coastal ecosystems: Eddy covariance hydrogen ion and oxygen exchange system (ECHOES). Limnol. Oceanogr.: Methods **13**: 438–450. doi:10.1002/lom3.10038

Long, M. H., J. E. Rheuban, D. C. McCorkle, D. J. Burdige, and R. C. Zimmerman. 2019. Closing the oxygen mass balance in shallow coastal ecosystems. Limnol. Oceanogr. **64**: 2694–2708. doi:10.1002/lno.11248

McGillis, W. R., C. Langdon, A. J. Williams, and B. Loose. 2009. O2-MAVS: An instrument for measuring oxygen flux. MTS/IEEE Biloxi - Marine Technology for Our Future: Global and Local Challenges, OCEANS 2009. 10.23919/oceans.2009.5422166

McGillis, W. R., C. Langdon, B. Loose, K. K. Yates, and J. Corredor. 2011. Productivity of a coral reef using boundary layer and enclosure methods. Geophys. Res. Lett. **38**: 2–6. doi:10.1029/2010GL046179

Middelburg, J. J., and L. A. Levin. 2009. Coastal hypoxia and sediment biogeochemistry. Biogeosciences **6**: 1273–1293. doi:10.5194/bg-6-1273-2009

Nepf, H. M. 2012. Flow and transport in regions with aquatic vegetation. Annu. Rev. Fluid Mech. **44**: 123–142. doi:10.1146/annurev-fluid-120710-101048

Owen, D. P., M. H. Long, W. K. Fitt, and B. M. Hopkinson. 2021. Taxon-specific primary production rates on coral reefs in the Florida keys. Limnol. Oceanogr. **66**: 625–638. doi:10.1002/lno.11627

Platz, M. C., Y. Takeshita, E. Bartels, and M. E. Arias. 2020. Evaluating the potential for autonomous measurements of net community production and calcification as a tool for monitoring coral restoration. Ecol. Eng. **158**: 106042. doi:10.1016/j.ecoleng.2020.106042

Rabouille, C., L. Denis, K. Dedieu, G. Stora, B. Lansard, and C. Grenz. 2003. Oxygen demand in coastal marine sediments: Comparing in situ microelectrodes and laboratory core incubations. J. Exp. Mar. Bio. Ecol. **285–286**: 49–69. doi:10.1016/S0022-0981(02)00519-1

Reidenbach, M. A., S. G. Monismith, J. R. Koseff, G. Yahel, and A. Genin. 2006. Boundary layer turbulence and flow structure over a fringing coral reef. Limnol. Oceanogr. **51**: 1956–1968. doi:10.4319/lo.2006.51.5.1956

Reidenbach, M. A., P. Berg, A. Hume, J. C. R. Hansen, and E. R. Whitman. 2013. Hydrodynamics of intertidal oyster reefs: The influence of boundary layer flow processes on sediment and oxygen exchange. Limnol. Oceanogr.: Fluids Environ. **3**: 225–239. doi:10.1215/21573689-2395266

Rheuban, J. E., P. Berg, and K. J. McGlathery. 2014. Ecosystem metabolism along a colonization gradient of eelgrass (*Zostera marina*) measured by eddy correlation. Limnol. Oceanogr. **59**: 1376–1387. doi:10.4319/lo.2014.59.4.1376

Ribberink, J. S. 1998. Bed-load transport for steady flows and unsteady oscillatory flows. Coast. Eng. **34**: 59–82. doi:10.1016/S0378-3839(98)00013-1

Rosman, J. H., and G. P. Gerbi. 2017. Interpreting fixed-location observations of turbulence advected by waves: Insights from spectral models. J. Phys. Oceanogr. **47**: 909–931. doi:10.1175/JPO-D-15-0249.1

Rovelli, L., K. M. Attard, L. D. Bryant, S. Flögel, H. Stahl, J. M. Roberts, P. Linke, and R. N. Glud. 2015. Benthic O_2 uptake of two cold-water coral communities estimated with the non-invasive eddy correlation technique. Mar. Ecol. Prog. Ser. **525**: 97–104. doi:10.3354/meps11211

Rowe, G. T., and others. 1988. Benthic carbon budgets for the continental shelf south of New England. Cont. Shelf Res. **8**: 511–527. doi:10.1016/0278-4343(88)90066-0

Scully, M. E., W. R. Geyer, and J. H. Trowbridge. 2011. The influence of stratification and nonlocal turbulent

production on estuarine turbulence: An assessment of turbulence closure with field observations. J. Phys. Oceanogr. **41**: 166–185. doi:10.1175/2010JPO4470.1

Sherwood, C. R., J. R. Lacy, and G. Voulgaris. 2006. Shear velocity estimates on the inner shelf off Grays Harbor, Washington, USA. Cont. Shelf Res. **26**: 1995–2018. doi:10.1016/j.csr.2006.07.025

Takeshita, Y., W. McGillis, E. M. Briggs, A. L. Carter, E. M. Donham, T. R. Martz, N. N. Price, and J. E. Smith. 2016. Assessment of net community production and calcification of a coral reef using a boundary layer approach. J. Geophys. Res. Oceans **121**: 5655–5671. doi:10.1002/2016JC011886

Tengberg, A., and others. 1995. Benthic chamber and profiling landers in oceanography—a review of design, technical solutions and functioning. Prog. Oceanogr. **35**: 253–294. doi:10.1016/0079-6611(95)00009-6

Tengberg, A., H. Stahl, G. Gust, V. Müller, U. Arning, H. Andersson, and P. O. J. Hall. 2004. Intercalibration of benthic flux chambers I. accuracy of flux measurements and influence of chamber hydrodynamics. Prog. Oceanogr. **60**: 1–28. doi:10.1016/j.pocean.2003.12.001

Trowbridge, J. H., and S. J. Lentz. 2018. The bottom boundary layer. Ann. Rev. Mar. Sci. **10**: 397–420. doi:10.1146/annurev-marine-121916-063351

Turk, D., and others. 2015. Community metabolism in shallow coral reef and seagrass ecosystems, lower Florida keys. Mar. Ecol. Prog. Ser. **538**: 35–52. doi:10.3354/meps11385

Volaric, M. P., P. Berg, and M. A. Reidenbach. 2018. Oxygen metabolism of intertidal oyster reefs measured by aquatic eddy covariance. Mar. Ecol. Prog. Ser. **599**: 75–91. doi:10.3354/meps12627

Acknowledgments

The authors thank Daniel McCorkle, Brian Hopkinson, and Kyle Conner for assistance with field work. This work was supported by NSF OCE grants 1657727 and 2023069.

Conflict of interest

None declared.

Submitted 25 August 2021
Revised 11 February 2022
Accepted 18 February 2022

Associate editor: John P Crimaldi